

Formation of ultracold dipolar molecules in the lowest vibrational levels by photoassociation

J. Deiglmayr^{a,b}, M. Repp^a, A. Grochola^{a,*}, K. Mörzlbauer^a, C. Glück^a, O. Dulieu^b, J. Lange^a, R. Wester^a, and M. Weidemüller^{a,†}

^a Physikalisches Institut Albert-Ludwigs-Universität Freiburg, Germany

^b Laboratoire Aimé Cotton, University Paris-Sud XI, Orsay, France

November 1, 2018

We recently reported the formation of ultracold LiCs molecules in the rovibrational ground state $X^1\Sigma^+, v''=0, J''=0$ [J. Deiglmayr *et al.*, PRL **101**, 133004 (2008)]. Here we discuss details of the experimental setup and present a thorough analysis of the photoassociation step including the photoassociation line shape. We predict the distribution of produced ground state molecules using accurate potential energy curves combined with an ab-initio dipole transition moment and compare this prediction with experimental ionization spectra. Additionally we improve the value of the dissociation energy for the $X^1\Sigma^+$ state by high resolution spectroscopy of the vibrational ground state.

1 Introduction

Ultracold molecular gases are promising candidates for studying diverse systems reaching from tests of the standard model to ultracold chemistry and quantum computing. Of special interest is the preparation of these molecules in the absolute rovibrational ground state, as this state is stable against inelastic collisions and allows therefore the creation of a stable, dense gas of molecules. A number of experimental approaches are currently being studied to prepare and manipulate ultracold molecules [1, 2]. Magneto-association using interspecies Feshbach resonances followed by adiabatic transfer via two or more optical transitions has been recently used to produce dense gases of deeply bound molecules of Cs₂ [3], KRb [4] and Rb₂ [5], even reaching the rovibrational ground state. Photoassociation (PA), a long established technique, has been successfully employed in the production of K₂ [6], RbCs [7], Cs₂ [8], and LiCs [9] in the lowest vibrational level of the electronic ground state. In contrast to the homonuclear molecules, heteronuclear alkali dimers exhibit strong dipole moments ranging from 0.6 Debye for LiNa and KRb to 5.5 Debye for LiCs [10]. The formation of these dipolar molecules in their lowest vibrational level opens the way to the exploration of quantum phases in

*Also at the Institute of Experimental Physics, Warsaw University, Poland

†e-Mail: weidemueller@physi.uni-heidelberg.de

dipolar gases [11, 12], the development of quantum computation techniques [13], precision measurements of fundamental constants [14], and the investigation and control of ultracold chemical reactions [15].

We recently reported the formation of ultracold LiCs molecules in the rovibrational ground state $X^1\Sigma^+, v''=0, J''=0$ [9]. In Sect. 2 of this article, we discuss details of the experimental setup with a special focus on the reduction of interspecies losses in overlapped magneto-optical traps. After analyzing the PA step and modeling the PA line shape in Sect. 3, we focus on the distribution of populated vibrational ground state levels in Sect. 4. In the discussion of the detection step, these predictions are compared with experimental ionization spectra and qualitative agreement is found (Sect. 5). Finally we present high-resolution spectroscopy of the vibrational ground state and improve the value of the dissociation energy of the lowest $X^1\Sigma^+$ level in Sect. 6.

2 Experimental setup

In this section, the experimental setup for the formation and detection of ultracold polar molecules is described. We outline the general principles and focus on recent important additions and improvements of the setup. Further details can be found in references [9, 16, 17].

2.1 Trapping a large number of atoms in overlapped magneto-optical traps

For the formation of dipolar ground state molecules, we cool and trap simultaneously ^7Li and ^{133}Cs atoms in two overlapped magneto-optical traps (MOTs). The atoms are evaporated in a double species oven and are decelerated in a single Zeeman slower*. In overlapped magneto-optical traps for different atomic species, high loss rates due to inelastic interspecies collisions are a well known experimental difficulty [18]. Fig. 1 a) demonstrates the importance of these losses for the setup used in previous experiments [16]. The dominant loss channel has been identified as collisions between excited $\text{Cs}(6P_{3/2})$ and ground state $\text{Li}(2S_{1/2})$ atoms [19]. It was therefore straightforward to reduce these losses by reducing the number of cesium atoms in the excited state. This was achieved by implementing a dark magneto-optical trap (also called “dark spontaneous force optical trap” or “dark SPOT” [20]) for cesium. In the center of such a trap, the repumping light is blocked, so that already cold atoms are pumped by the cooling light off-resonantly into the lower hyperfine ground state which is now a dark state. Only if they leave the central part of the trap, they are pumped back by repumping light and take part in the cooling cycle again. This has been widely used to increase number and density of the trapped atoms (which we also observe), however we mainly profit from the large fraction of atoms in the dark hyperfine ground state (typically 97%) which reduces interspecies loss-rates by the same fraction. The repumping light in the center is blocked by imaging the shadow of a 3.5mm large piece of plastic† with

*When both traps are loaded simultaneously, the configuration of the Zeeman fields is optimized for slowing lithium atoms. With this field configuration, the loading rate for cesium atoms is reduced to 1×10^7 atoms/s which is still sufficient for the experiments described here.

†It turned out that the best extinction ratio of $1:10^4$ at the trap position was obtained by using the magnetic plastic from an old floppy disk.

an 1:1 telescope onto the trap center. As the laser beam used for Zeeman-slowing of the atoms also contains repumping light and passes through the center of the trap, we additionally image a dark spot (also 3.5mm, 1:1 imaging ratio) in the Zeeman beam onto the trap center. The Rayleigh range of the imaging focus is on the order of only a few centimeters, so that the slowing of the atomic beam is not significantly reduced by the shadow in the center of the Zeeman beam. We note that the reduced absolute power in the Zeeman beam leads to a reduced loading rate which is however more than compensated by the reduced single species losses in a dark SPOT. In order to reach a high dark-state fraction, we detune the repumping laser by $\sim 5\Gamma$ and shine an additional depumping laser on the center of the trap ($100\mu\text{W}$, $\omega_0=1.5\text{mm}$). This setup is called a detuned forced dark SPOT [21]. Fig. 1 b) demonstrates the increase in the number of simultaneously trapped lithium and cesium atoms after implementing the detuned forced dark SPOT for cesium. With this setup we typically trap 4×10^7 Cs atoms and 10^8 Li atoms at densities of $3 \times 10^9 \text{cm}^{-3}$ and 10^{10}cm^{-3} respectively. Using absorption images and time-of-flight expansion we measure a Cs temperature of $250(50)\mu\text{K}$. The temperature of the Li atoms lies significantly higher (hundreds of μK) due to the unresolved hyperfine structure of the excited state and the large photon recoil.

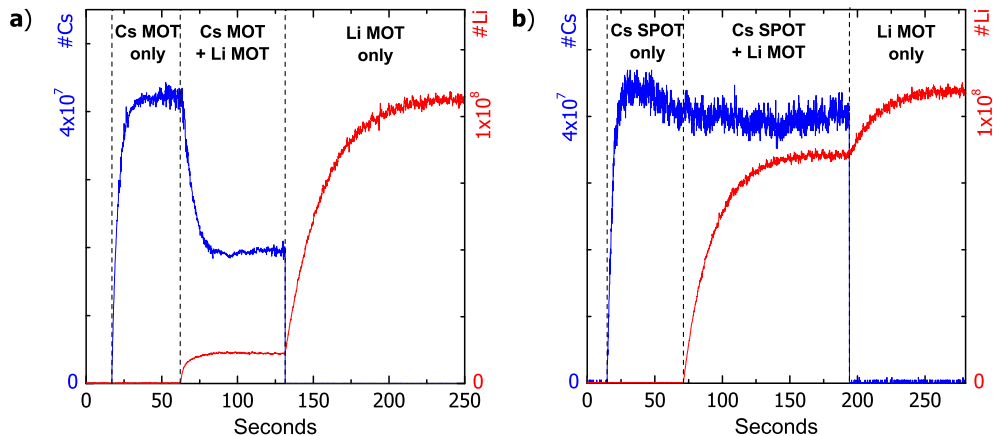


Figure 1: Loading curves for overlapped lithium and cesium traps: a) First only the cesium MOT is loaded, then additionally the lithium MOT. The number of trapped cesium atoms is reduced by roughly a factor of two. After blocking the cesium MOT, roughly a 9-fold increase in the number of trapped lithium atoms is observed, indicating very high losses due to Li-Cs collisions. b) The same sequence with overlapped forced dark SPOT for cesium and identical lithium MOT. Only a weak suppression of trapped atom numbers is observed when loading both traps simultaneously.

2.2 Molecule production and detection

In order to form ultracold molecules, colliding pairs of laser cooled atoms are transferred into bound molecules by photoassociation (PA) [22]. Light from a tunable laser is continuously shown on the overlapped atomic clouds. Two colliding atoms can absorb

a photon from this laser and form an excited bound molecule. The spontaneous decay of these excited molecules can either lead back to pairs of free atoms (usually with additional kinetic energy) or into bound molecules in the lowest singlet or triplet state. In the system described here, the latter is the dominant process as it will be shown later (Sect. 4). The light for the PA is provided by a commercial Ti:Sa laser (Coherent MBR-110, pumped by 9 to 12 Watts from a Coherent Verdi V18) and is delivered to the UHV chamber by a high power optical fibre. After the fibre, the light is collimated to a waist of 1.0mm, matched to the size of the lithium MOT. It is aligned to pass through the center of the overlapped cesium and lithium MOT's by optimizing the depletion of trapped cesium atoms with resonant light from the Ti:Sa laser. Typical laser powers after the chamber are 400-500mW for wavelengths between 946 and 852nm. The wavelength is measured using a home-built wavemeter, calibrated to an atomic cesium resonance with an absolute accuracy of 0.01 cm^{-1} . Additionally we monitor Ti:Sa frequency scans with a reference cavity, which is stabilized via an offset-locked diode laser to an atomic cesium resonance. This reference cavity is also used for monitoring long-term drifts of the Ti:Sa laser and to lock it to an arbitrary frequency with a remaining fluctuation of $\lesssim 2\text{MHz/day}$.

In order to detect the produced ground state molecules, they are first ionized state-selectively by a pulsed laser. The resulting LiCs^+ ions are then separated by time-of-flight mass spectrometry from other atomic or molecular ions and are finally detected on a microchannel plate in a single ion counting setup. For details of the time-of-flight mass spectrometer we refer to a previous work [16]. We only note that it allows us to clearly separate Cs^+ ions from LiCs^+ ions which have a mass difference of 5%. For ionization, two photons of one color from a pulsed dye laser (Radiant Dyes NarrowScan, Rhodamin B/6G pumped by 532nm, typically 4mJ in a beam with a waist of 5mm and a pulse length of 7ns, bandwidth 0.1cm^{-1}) are used in a resonant-enhanced multiphoton ionization (REMPI) scheme. The pulsed laser beam passes roughly one beam diameter below the trapped atom clouds in order to reduce excessive ionization of cesium and lithium atoms which would saturate the detector. Additionally the number of cesium ions is reduced by turning off the repumping light 0.6ms before the ionization pulse. The depumper used in the forced dark-spot setup quickly pumps all trapped cesium atoms into the lower hyperfine state $F=3$, so that the trapping laser is now off-resonant and the atoms remain in the electronic ground state from where only three photon ionization is possible. In contrast to two-photon ionization from the excited $6P_{3/2}$ state, this process is strongly suppressed and therefore the possible effect on the detected LiCs^+ signal is minimized. After the ionization pulse the repumper is turned on again within $300\mu\text{s}$ and nearly all cesium atoms are recaptured in the MOT.

3 Photoassociation spectroscopy

In Fig. 2 we show an individual resonance in a scan of the PA laser. As the PA laser becomes resonant with a transition from a colliding atom pair to an excited molecular level, the number of detected LiCs^+ ions increases, indicating the formation of ground state molecules. We can indeed be sure that the ion signal arises from ground state molecules and not from excited molecules, as the PA and ionization laser are spatially separated and the molecules do not move significantly over the lifetime of the excited level. We note, however, that in these first experiments the wavelength of the ionization laser was chosen based on a rough estimate only, relying on *ab initio* potentials for the

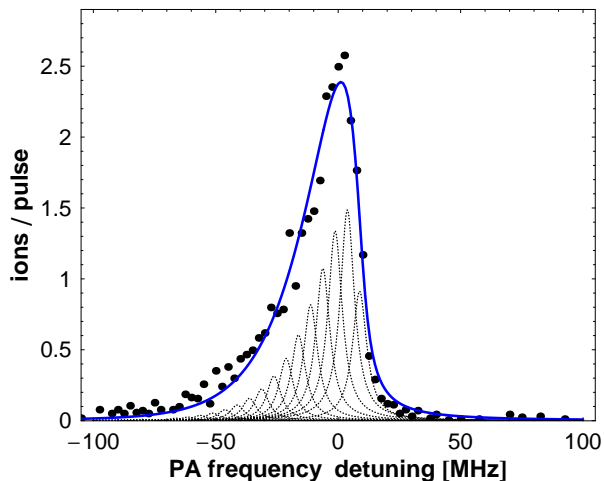


Figure 2: Temperature-broadened PA resonance (dots) together with a fit of Equation (1) (solid line). Best fit parameters are $T_{rel}=580(80)\mu\text{K}$ and $\Gamma=10(3)\text{MHz}$. The thin dashed lines illustrate the contribution to the PA line shape from atom pairs with discrete collision energies. The frequency axis shows detuning from the setpoint of 11632.11cm^{-1} . The molecules are ionized by two photons at 14693.7cm^{-1} .

intermediate levels and for the ion potential. The precise ionization mechanism at wavelengths around 14700cm^{-1} is still under investigation.

The resonance shown in Fig. 2 does not show further substructure, i.e. no molecular hyperfine structure, indicating zero electronic angular momentum and therefore an $\Omega=0^{+/-}$ character. As only a single rotational component was observed for this line, no further assignment is possible. Nevertheless an accurate analysis of the PA line shape can yield important information about the atomic scattering state. More specifically, the asymmetric broadening of the line towards red detunings indicates the influence of the collision energy on the PA line shape and can therefore be used as a measure for the relative temperature of the two species. As discussed by Jones *et al.* [23], an accurate model of PA lines shapes can be derived from Wigner’s law. It states that for low collision energies ε the amplitude of the scattering wavefunction with angular momentum ℓ scales as $\varepsilon^{(\ell+1/2)/2}$. With the probability to have a collision with energy ε given by the Boltzmann factor $e^{-\varepsilon/T}$, the shape of a PA resonance is then described by

$$W_i(f, f_0) = B \int_0^\infty e^{-\varepsilon/T} \varepsilon^{(\ell+1/2)} L_\Gamma(f, f_0 - \varepsilon) d\varepsilon, \quad (1)$$

where $L_\Gamma(f, f_0)$ is the discrete energy Lorentzian with natural linewidth γ and central frequency f_0 . Fig. 2 shows the temperature broadened PA resonance together with a fit of the model from Eq. (1) taking only s-wave scattering ($\ell=0$) into account. The fit yields realistic values for $T=580(80)\mu\text{K}$ and $\Gamma=10(3)\text{MHz}$. Adding higher partial waves did not improve the fit.

Jones *et al.* also derive a limit on the collision energy ε , for which the Wigner law

holds:

$$\frac{h\varepsilon}{k_B} \ll \frac{E_{col}}{k_B} \frac{2}{(0.6 - A_0/R_0)^2}$$

where

$$R_0 = \left(\frac{2\mu C_6}{\hbar^2} \right)^{1/4} \quad \text{and} \quad E_0 = \frac{\hbar}{2\mu R_0^2}.$$

For ${}^7\text{Li}{}^{133}\text{Cs}$ the reduced mass μ and the C_6 dispersion coefficient [24] are well known. However there are only two experimental values for the scattering length A_0 , namely $A_{0,\text{singlet}}=50(20)a_0$ from high-resolution spectroscopy of the singlet ground state potential [25] and $A_{0,\text{eff}}=180(40)a_0$ from the thermalization of ${}^7\text{Li}$ and ${}^{133}\text{Cs}$ atoms in an optical dipole trap [26]. While the first value yields an upper limit of roughly 0.8K well above our experimental conditions, the latter one yields 1.7mK closer to the fitted temperature. As a second condition the long-range wavefunction of the ground state has to be linear near the outer turning point of the PA level. The PA for the fitted resonance was performed at a detuning of more than 100cm^{-1} from the asymptote where the excited potential energy curve is still quite steep. Therefore the vibrational wavefunction is very localized at the outer turning point and this second condition should be well fulfilled. We conclude that if the relevant scattering length for our experiment lies between $A_{0,\text{singlet}}$ and $A_{0,\text{eff}}$, the derived collision energy of $T=580(80)\mu\text{K}$ should be a realistic estimate for our experimental conditions.

This relatively high temperature has to be seen in relation to the centrifugal barrier E_ℓ for collisions with higher angular momentum ℓ :

$$E_\ell = \left(\frac{\hbar^2 \ell(\ell+1)}{3\mu(2C_6)^{1/3}} \right)^{3/2}. \quad (2)$$

For p -wave scattering this yields $E_{\ell=1}=1.6\text{mK}$ (barrier peaked at $103a_0$), for d -wave scattering $E_{\ell=2}=8.5\text{mK}$ (barrier peaked at $78a_0$), and for f -wave scattering $E_{\ell=3}=24.7\text{mK}$ (barrier peaked at $66a_0$). Our measured collision temperature is well below the p -wave limit, so that one can expect to observe dominantly s -wave scattering. Assuming a Boltzmann distribution of kinetic energies, in roughly 6% of the collisions the energy lies above the p -wave barrier, so that we can expect a small contribution from $\ell=1$ but none from higher partial waves.

Using the above measured value of the collision temperature, we can draw further conclusions about the temperature of the lithium atoms and give an estimate on the temperature of the formed molecules. As a simple approximation we assume an average collision angle between lithium and cesium atoms of 90° . The relative kinetic energy is then given by $E_{rel} = \frac{1}{2} \frac{m_{Li} m_{Cs}}{m_{Li} + m_{Cs}} (v_{Li}^2 + v_{Cs}^2)$ and therefore the relative temperature $T_{rel} = \frac{m_{Cs} T_{Li} + m_{Li} T_{Cs}}{m_{Li} + m_{Cs}}$ is dominated by the lighter lithium. Solving this equation for T_{Li} with $T_{Cs}=250\mu\text{K}$ and $T_{rel}=580\mu\text{K}$ yields $T_{Li}=600\mu\text{K}$, which seems reasonable. For the center of mass motion of the formed molecules $E_{c.m.} = \frac{1}{2} (m_{Li} + m_{Cs}) \left(\frac{m_{Li} \vec{v}_{Li} + m_{Cs} \vec{v}_{Cs}}{m_{Li} + m_{Cs}} \right)^2$. Therefore the molecular temperature $T_{c.m.} = \frac{m_{Li} T_{Li} + m_{Cs} T_{Cs}}{m_{Li} + m_{Cs}}$ is dominated by the heavier cesium. From the above determined temperature T_{Li} and T_{Cs} we calculate a molecular temperature of $270(60)\mu\text{K}$.

3.1 Photoassociation into the $B^1\Pi$ state

The effort of searching for PA resonances especially at large detunings can be substantially reduced when spectroscopic information on the excited states of the system under

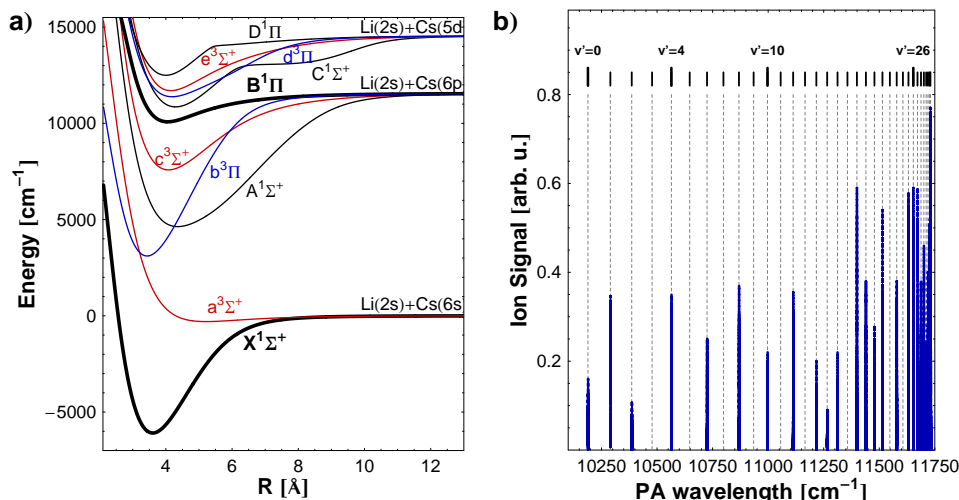


Figure 3: a) Potential energy curves for Σ^+ and Π states of LiCs correlating to the three lowest asymptotes. The relevant states $B^1\Pi$ and $X^1\Sigma^+$ are marked bold. b) Overview over all observed vibrational levels in the $B^1\Pi$ state.

investigation is available. Most experimentally determined potential energy curves are based on the observation of absorption and fluorescence between bound levels, leading to a relative uncertainty on the order of 0.01 cm^{-1} in addition to an uncertainty of the dissociation energy of the molecular ground state of up to 1 cm^{-1} and therefore a corresponding uncertainty in the PA wavelength which refers to the atomic asymptote. Once however a few levels have been observed and assigned, this dissociation energy is known with high precision and all other levels can be found easily. If no spectroscopic data is available, *ab initio* calculated molecular potentials can be helpful. With up-to-date methods, the typical uncertainty of the calculated potentials is on the order of 100 cm^{-1} , while the vibrational spacings, related to the shape of the potentials, are determined much more precisely. Therefore, *ab initio* potential curves provide a good estimate of the typical number of expected PA resonances in a given energy range, with an uncertainty for hitting one of them on the order of the vibrational spacing. Once a vibrational progression is observed, they are of importance for the final assignment and the prediction of further vibrational levels.

In Fig. 3 a) *ab initio* curves for selected electronic states of LiCs correlating to the lowest three asymptotes are shown (spin-orbit coupling is neglected in this calculation). For two excited states, the $B^1\Pi$ and the $D^1\Pi$ state, Stein *et al.* have published potential curves derived from high resolution laser-induced fluorescence spectroscopy [27]. They report strong perturbations of the rovibrational levels in the $D^1\Pi$ state due to spin-orbit coupling to nearby triplet states. These perturbations reduce the probability for decay into the lowest singlet state and also reduce the accuracy of an extrapolation from the highly excited rotational levels observed in Ref. [27] to the lowest rotational levels addressable by PA. In contrast to the $D^1\Pi$ state, the $B^1\Pi$ state showed no significant

perturbations, allowing for an extrapolation of level energies to low rotational states with high precision and making the spontaneous decay into the $X^1\Sigma^+$ ground state more likely. For the formation of ground state molecules we therefore focused on the $B^1\Pi$ state. Extensive PA scans were performed and PA resonances corresponding to rovibrational levels in $B^1\Pi$ from the atomic asymptote down to $v'=0$ at $\sim 1540\text{cm}^{-1}$ detuning from this asymptote were observed. For levels below $v'=25$ we found very good agreement with the energies reported in Ref. [27]. As the authors of the cited work could only extrapolate from the last observed level around $v'=25$ towards the asymptote, the predictions became less accurate as we approached the asymptote. Here additional vibrational levels up to $v'=35$ were found, yielding a data set for the $B^1\Pi$ state with level energies ranging from the bottom of the potential at $v'=0$ up to the last level below the asymptote, bound only by ~ 1 GHz. A publication describing the complete $B^1\Pi$ potential energy curve is in preparation [28]. We note that we did not observe line broadening due to predissociation in the region between the fine structure asymptotes $\text{Li}(2^2S_{1/2})+\text{Cs}(6^2P_{3/2})$ and $\text{Li}(2^2S_{1/2})+\text{Cs}(6^2P_{1/2})$ as suggested by Ref. [27]. We are currently studying theoretically and experimentally in how far predissociation could be relevant for other electronic states correlated to the upper asymptote $\text{Li}(2^2S_{1/2})+\text{Cs}(6^2P_{3/2})$ [29].

In Fig. 3 b) an overview over all observed PA resonances in the $B^1\Pi$ state is given. It is not straightforward to compare the strength of the different PA lines, as not all PA resonances could be detected at the same ionization wavelength and the ion yield additionally strongly depends on the populated ground state levels which vary between different PA resonances. However the observed rate of molecule formation for PA into deeply bound vibrational levels of $B^1\Pi$ is surprisingly high, as these transitions occur at very short internuclear separations around $R=4\text{\AA}$ where the amplitude of the free scattering wavefunction is already greatly reduced. It is noteworthy, that the Condon-points of these deeply bound levels coincide with the inner turning point of the $a^3\Sigma^+$ potential, which could be an important clue towards a full explanation of the observed high PA rates.

The observed PA resonances in the $B^1\Pi$ state show a rich substructure due to molecular hyperfine interactions as expected for a state with electronic angular momentum. Exemplary resonances are shown in Fig. 4. The observed hyperfine splitting generally decreases with increasing J' . We do not expect to observe broadening of the lines due to stray fields, as the electric extraction fields for the detection are switched on only $500\mu\text{s}$ before the dye laser pulse, which ionizes all molecules that have been produced within the last 20ms. Therefore the PA is performed mainly under electric-field-free conditions. Also magnetic fields should not influence the measured PA spectra. The magnetic field gradient for trapping the atoms is applied constantly, but residual fields in the trap center (where the gradient field reaches zero) have been compensated to <1 Gauss.

For low lying levels $v'<25$, rotational components $J'=1$ and 2 were observed, for levels $v'\geq 25$ a weaker $J'=3$ component and for the last bound levels rotational components up to $J'=5$ were visible. As the Condon-points for even the last bound levels lie well within the centrifugal barrier for higher angular momenta in the scattering continuum, the higher rotational components are unlikely to be due to PA from atom pairs with higher angular momentum. The observation of these higher J components is probably due to the change of coupling between angular momenta as the molecules become less tightly bound. From Fig. 4 one can further learn, that while for the higher

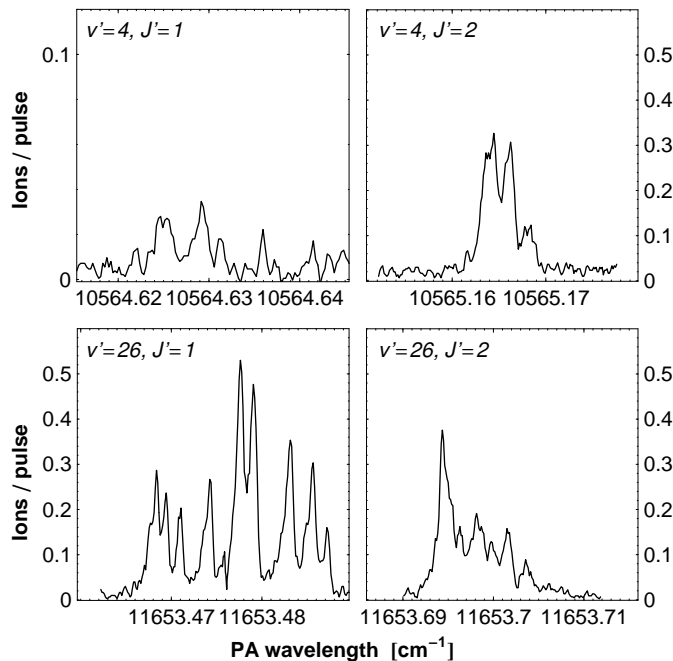


Figure 4: Photoassociation resonances for different rovibrational levels $B^1\Pi, v', J'$. Abscissas and ordinates are on the same scale for all panels except for $v'=4, J'=1$, where the signal is scaled by a factor of 5 for visibility.

lying state the $J'=1$ component is the stronger one, for $v'=4$ the $J'=2$ component is clearly dominant. This also indicates a change in the free-bound coupling from PA at short distances around 5\AA to PA at larger internuclear separations around 9\AA which is currently under investigation.

4 Calculated probabilities for decay into the $X^1\Sigma^+$ state

After PA, the formed excited molecules decay within a few nanoseconds either into bound molecules or into free atom pairs. In order to estimate the branching ratio between these two competing channels and to predict the distribution of populated vibrational ground state levels, we calculated Franck-Condon factors and Einstein-A coefficients for transitions between the excited and the ground state levels.

As mentioned before, accurate experimental potential energy curves have been published for the $X^1\Sigma^+$ state [25] and for vibrational levels $v' \leq 25$ of the $B^1\Pi$ state [27] of $^7\text{Li}^{133}\text{Cs}$. The authors of the latter paper included our observed PA resonances in the fit describing the full potential energy curve of the $B^1\Pi$ state [30], yielding very accurate potential energy curves covering all binding energies. We calculate rovibrational levels in these potentials using the mapped Fourier grid Hamiltonian (FGH) method,

which is used to solve numerically the time-independent radial Schrödinger equation. A detailed description of the method may be found elsewhere [31]. As expected, the resulting term energies are in very good agreement with experimental observations (residuals $\leq 0.02\text{cm}^{-1}$). These transition energies are used in the identification of ionization resonances (Sect. 5) and depletion resonances (Sect. 6). The resulting wavefunctions are used to calculate Franck-Condon (FC) factors for the bound-bound transitions. It is worth mentioning, that for excited states $B^1\Pi, v' \leq 26$ the sum of FC factors with all vibrational levels of the ground state is close to unity. Molecules in these $B^1\Pi$ levels will therefore predominantly decay into bound molecular ground state levels. We also note, that the authors of Ref. [27] report only for levels $v' \geq 17$ observation of weak decay into the $a^3\Sigma^+$ lowest triplet state. One can therefore expect, that levels $B^1\Pi, v' < 17$ decay almost completely towards $X^1\Sigma^+$ levels and that higher levels exhibit only a weak additional decay channel towards $a^3\Sigma^+$ levels.

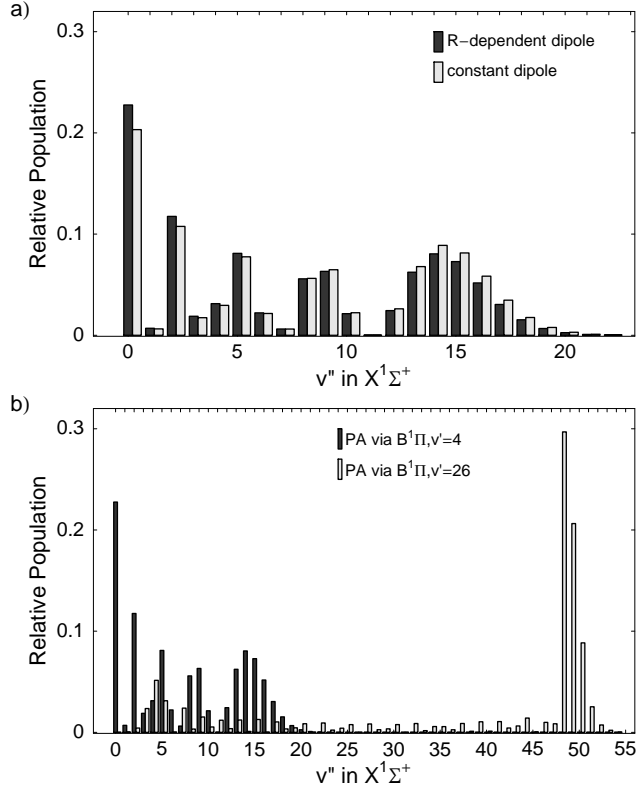


Figure 5: Calculated $X^1\Sigma^+$ level populations after PA, normalized to unity: a) influence of the R-dependence of the transition dipole moment on the expected distribution after PA via $B^1\Pi, v'=4$; b) comparison of the expected level population after PA via $B^1\Pi, v'=4$ and $v'=26$.

Using the approach described in Ref. [10], the R -dependent dipole transition mo-

ment $\mu(R)$ was calculated for the electronic transition $X^1\Sigma^+-B^1\Pi$. The transition dipole moment does not vary more than 10% from a value of 9.9 Debye over the relevant range of distances. By calculating the Einstein A coefficients for spontaneous decay $A_{ij} = \frac{2}{3} \frac{\omega_{ij}^3}{\epsilon_0 \hbar c^3} |\langle \Psi_i | \mu(R) | \Psi_j \rangle|^2$ with ω_{ij} being the transition frequency and Ψ_i the nuclear wavefunction of the vibrational level i , one can derive the relative population of ground state vibrational levels after PA via different excited states. In Fig. 5 b) the normalized population of $X^1\Sigma^+$ levels after PA via $B^1\Pi, v'=4$ and $B^1\Pi, v'=26$ is compared. While in both cases low lying vibrational levels are populated, we note that after PA via $B^1\Pi, v'=4$, more than 20% of the excited molecules should decay into the lowest vibrational level $v''=0$. Fig. 5 a) shows the small influence of a calculation with the R-dependent versus a constant dipole moment function for this calculation.

5 Ionization spectroscopy of $X^1\Sigma^+$

The formation of ground state molecules is probed by ionizing those molecules via resonantly-enhanced multiphoton ionization (REMPI) and subsequent detection of the molecular ions (see Sect. 2.2). Once the formation of molecules by the PA laser has been detected, a scan of the ionization laser yields information about the distribution of populated vibrational levels. Extracting this information requires accurate knowledge of the involved ground and intermediate electronic states. In the case of LiCs, deeply bound $X^1\Sigma^+$ levels $v'' \leq 4$ can be ionized via intermediate levels in the $B^1\Pi$ state which allows us to assign observed ionization resonances to ground and intermediate state vibrational levels.

As discussed in the previous section, different PA resonances are expected for different relative populations of ground state levels. This can be seen very clearly in the three REMPI scans of Fig. 6 covering the same range of ionization energies after PA via different levels in the $B^1\Pi$ state. Although the assignment of resonances to ground state levels is often ambiguous and a number of unpredicted resonances indicate the importance of intermediate states other than $B^1\Pi$, quite a few clear progressions are visible. In Fig. 6 a), resonances from $X^1\Sigma^+, v''=0$ to $B^1\Pi, v'=13-17$ and $X^1\Sigma^+, v''=2$ to $B^1\Pi, v'=17-21$ can be identified; in Fig. 6 b), in addition to the resonances originating from $v'' = 2$, resonances from $X^1\Sigma^+, v''=1$ to $B^1\Pi, v'=14-21$ are visible; and in Fig. 6 c), in addition to molecules in $v''=1$ and $v''=2$, also molecules in $v''=3$ are ionized through $B^1\Pi, v'=22-29$. The appearance of these ‘‘ionization windows’’ in the intermediate $B^1\Pi$ state demonstrates the importance of the bound-bound transition dipole moment and the level-dependent ionization probability of the $B^1\Pi$ state which lead to a selection of ionization pathways.

The different and unknown ionization probabilities for different intermediate $B^1\Pi$ levels as well as near degeneracy of many transitions complicate an analysis of the relative populations of vibrational ground state levels from the observed ionization spectra. However, as shown in Fig. 7, we can establish at least a qualitative agreement with the predictions of Sect. 4. In Fig. 7, the average peak value for each of the above identified transition bands originating from ground state levels $v''=0-3$ is shown. While the unknown ionization probabilities of intermediate levels impede the direct extraction of the level population from the measured spectra, we can still deduce the population strength of a single level after PA via different excited levels and compare it with our prediction. As can be seen in Fig. 7, the relative ordering of the line strengths for

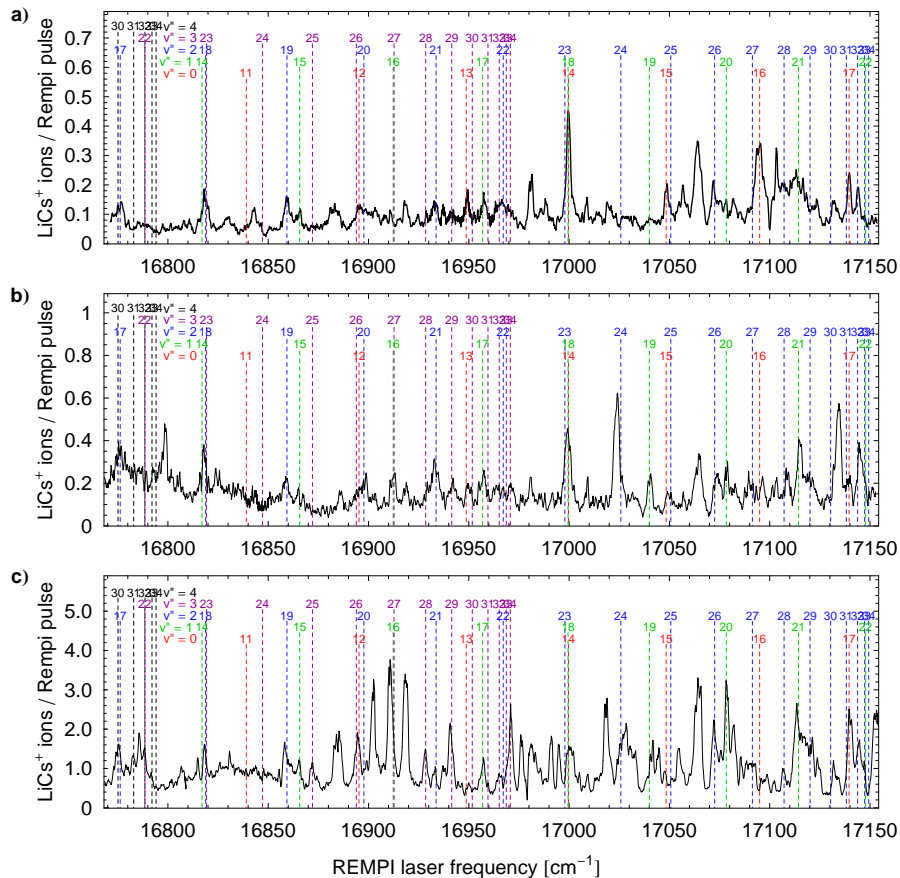


Figure 6: Resonantly-enhanced two-photon ionization spectra of ground state molecules after photoassociation via a) $B^1\Pi, v'=4, J'=2$, b) $v'=10, J'=2$, and c) $v'=26, J'=2$ over the same range of ionization energies. In the upper part of the graph, expected transitions series originating from all levels v'' in $X^1\Sigma^+$ to all levels v' in $B^1\Pi$ are marked (note that this can not yield a full assignment of the observed lines, as different ionization probabilities and other intermediate states are neglected). Wavelengths calibrated with a High Finesse WS7 wavemeter with an accuracy $\ll 0.1\text{cm}^{-1}$.

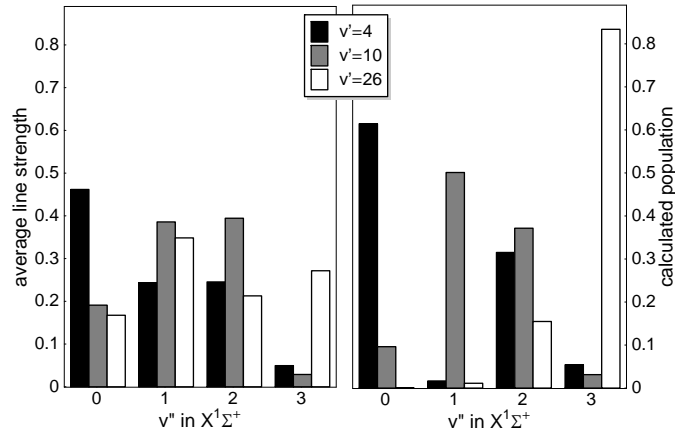


Figure 7: Comparison of detected ground state levels for different photoassociation resonances with predictions. Left panel: averaged peak value for the transition bands originating in $X^1\Sigma^+, v'=0-3$ as discussed in the text (normalized to unity for every PA resonance); Right panel: calculated ground state population, normalized to the summed population in levels $v'=0-3$ (see Sect. 4).

each level v'' is described correctly by the theory, while the relative ratios show strong deviations. This is very likely due to saturation and a non-optimal signal-to-noise level.

The identification of the observed ionization resonances also yields information about the lowest state of the ion LiCs^+ , the $X^2\Sigma^+$ state. The energy of two photons from $X^1\Sigma^+, v''=0$ (via intermediate level $B^1\Pi, v'=13$) leads to ionization at a detuning of -3385cm^{-1} from the $\text{Li}(2^2S_{1/2})+\text{Cs}^+(^1S_0)$ threshold at 31406.71cm^{-1} [32]. Therefore the $X^2\Sigma^+$ state of the ion has a depth of at least 3385cm^{-1} , favoring the predictions of Von Szentpaly ($D_e=3468\text{cm}^{-1}$ [33]), Korek ($D_e=3578\text{cm}^{-1}$ [34]), and Azizi ($D_e=3564\text{cm}^{-1}$ [35]) over calculations of Patil ($D_e=2662\text{cm}^{-1}$ [36]) and Bellomonte ($D_e=2984\text{cm}^{-1}$ [37]).

6 High resolution spectroscopy of the vibrational ground state

After having identified vibrational ground state levels by selective ionization of these levels, we can further probe the formed ground state molecules by applying depletion spectroscopy [38]. While the Ti:Sa laser is stabilized to a PA resonance (see Sec. 3) and the pulsed dye laser is kept on resonance for the ionization of a certain ground state level, a narrow band laser is used to optically pump the molecules out of this specific level and therefore reduce the number of detected ions. As this laser (Radiant Dyes cw dye laser, Rhodamin 6G pumped at 532 nm) has a bandwidth on the order of a few MHz, it allows one to resolve rotational transitions between ground and excited molecular states. The light from the laser is coupled into a fibre and, after being

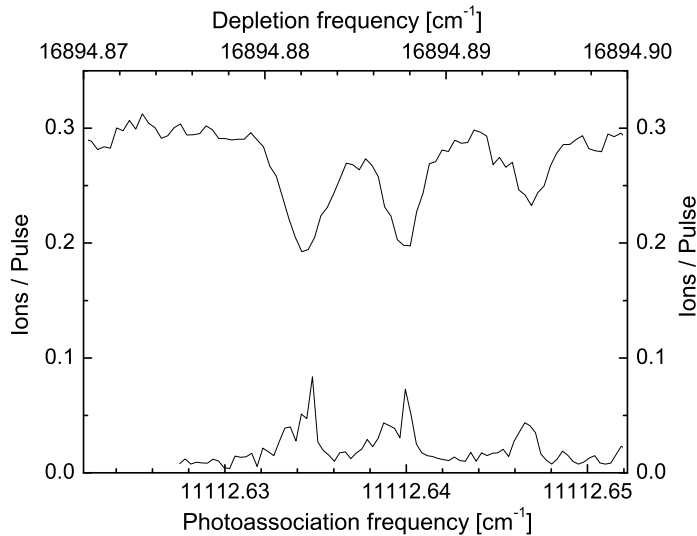


Figure 8: Depletion scan of $X^1\Sigma^+, v''=0, J''=2$ molecules via $B^1\Pi, v'=12, J'=1$ (upper trace) aligned to a photoassociation scan of the same excited level (lower trace). Depletion laser intensity 26 mW/cm^2 , photoassociation laser intensity 25 W/cm^2 . Molecules detected at different ionization wavelengths.

collimated to a waist of 0.7 mm , is aligned collinear with the PA-laser by maximizing the depletion of the ion signal on resonance. The frequency of this laser is measured with a wavemeter (Burleigh WA-1000, relative stability 500 MHz) and scans are monitored additionally with a reference cavity (FSR= 750 MHz), which is actively stabilized to an atomic cesium resonance via an offset-locked diode laser. This high resolution spectroscopy of ground state molecules allowed us to confirm assignments made in the interpretation of REMPI spectra and to confirm the production of $X^1\Sigma^+, v''=0$ molecules after a single PA step [9].

The depletion spectroscopy makes it possible to gain further information about the $X^1\Sigma^+$ potential energy curve. As shown in Fig. 8, the $B^1\Pi, v'=12, J'=1$ level was observed in PA spectroscopy starting from the $\text{Li}(2^2S_{1/2}, F=2) + \text{Cs}(6^2S_{1/2}, F=3)$ asymptote as well as in depletion spectroscopy starting from $X^1\Sigma^+, v''=0, J''=2$. Using the calculated rotational constant $B_{v''=0} = 0.1874 \text{ cm}^{-1}$ for the ground state, this allows us to give a hyperfine averaged value for the binding energy of the lowest vibrational level $D_0^X = 5783.53(3) \text{ cm}^{-1}$. This agrees within the errorbars with the value of $D_0^X = 5783.4(1) \text{ cm}^{-1}$ given by Staunum *et al.* [25].

7 An efficient route towards a dense gas of absolute ground state molecules

In this article we have discussed in detail the steps in the formation and detection of ultracold polar LiCs molecules in the vibrational ground state. We have shown that a single absorption-emission cycle is sufficient to produce the molecules in the lowest

vibrational state. Previously we have demonstrated also the formation of ultracold LiCs molecules in the rotational and vibrational ground state $X^1\Sigma^+, v''=0, J''=0$ [9] in a single step of PA. In the future we will repeat these experiments with lithium and cesium atoms trapped in a quasi-electrostatic trap (QUEST) formed by a focused CO_2 laser at $10.6\mu\text{m}$. This very large detuning from any atomic or molecular resonance makes the absorption of a trap laser photon by LiCs molecules very unlikely: a transition from deeply bound molecules into the first excited state requires roughly ten photons from the trap laser. Due to the permanent dipole moment of the polar molecules, transitions within an electronic state are in principle also possible; however, they are very unlikely due to extremely small Franck-Condon overlaps for such transitions.

From a calculation of the static polarizability of LiCs molecules in $X^1\Sigma^+, v''=0$ [39] and previous results obtained with this setup [40], we expect a trap depth on the order of $600\mu\text{K}$ for the ground state molecules in $v''=0$. The calculation shows, that the trap depth increases for higher vibrational levels, so that all produced ground state molecules are expected to be trapped. While the molecules in $v''=0, J''=0$ are expected to be stable against collisions with other atoms and molecules in the same state, collisions with vibrationally excited molecules can lead to a loss of $v''=0$ molecules. It will therefore be useful to apply the PA laser only as long as the number of atoms in the trap significantly exceeds the number of produced molecules, in which case any molecule would most likely collide with a trapped atom and not with a molecule. As demonstrated for Cs_2+Cs collisions [41, 42] and $\text{RbCs}+\text{Cs}/\text{Rb}$ collisions [43], such collisions lead to a fast removal of vibrationally excited molecules from the trap. After an accumulation time on the order of seconds, one would end up with a relatively pure sample of molecules in the rovibrational ground state. Optimistically, 20% of the trapped atoms could be transferred into molecules in the rovibrational ground state. Starting from atomic densities on the order of 10^{11}cm^{-3} and atomic temperatures around $20\mu\text{K}$ [26], one can therefore hope to reach molecular samples with densities on the order of 10^{10}cm^{-3} and temperatures also around $20\mu\text{K}$. While this is far away from a degenerate gas of polar molecules, the long-range dipolar interactions will already at these densities lead to a strongly interacting system. After stabilizing the polar gas against inelastic collisions due to these interactions, *e.g.* via a “blue shield” for molecules [44] or by preparing aligned, 2-dimensional samples in combined static electric fields and strong laser fields [39], the realization of a new quantum phase like a dipolar crystal [12] seems feasible.

Acknowledgements: We thank S.D. Kraft and P. Staunum for contributions at the early stage of the experiment. We also thank E. Tiemann and A. Pashov for providing experimental LiCs potentials before publication and, together with J. Hutson, for fruitful discussions. This work is supported by the DFG under WE2661/6-1 in the framework of the Collaborative Research Project QuDipMol within the ESF EURO-CORES EuroQUAM program. JD acknowledges partial support of the French-German University. AG is a postdoctoral fellow of the Alexander von Humboldt-Foundation.

References

- [1] J. Doyle, B. Friedrich, R. V. Krems, and F. Masnou-Seeuws, *Eur. Phys. J. D*, 2004, **31**, 149.
- [2] O. Dulieu, M. Raoult, and E. Tiemann, *J. Phys. B*, 2006, **39**, Introductory review.
- [3] J. G. Danzl, E. Haller, M. Gustavsson, M. J. Mark, R. Hart, N. Bouloufa, O. Dulieu, H. Ritsch, and H.-C. Nägerl, *Science*, 2008, **321**, 1062; H.-C. Nägerl *private communication*.
- [4] K.-K. Ni, S. Ospelkaus, M. H. G. de Miranda, A. Pe'er, B. Neyenhuis, J. J. Zirbel, S. Kotochigova, P. S. Julienne, D. S. Jin, and J. Ye, *Science*, 2008, **322**, 231.
- [5] F. Lang, K. Winkler, C. Strauss, R. Grimm, and J. H. Denschlag, *Phys. Rev. Lett.*, 2008, **101**, 133005.
- [6] A. N. Nikolov, J. R. Ensher, E. E. Eyler, H. Wang, W. C. Stwalley, and P. L. Gould, *Phys. Rev. Lett.*, 2000, **84**, 246.
- [7] J. M. Sage, S. Sainis, T. Bergeman, and D. DeMille, *Phys. Rev. Lett.*, 2005, **94**, 203001.
- [8] M. Viteau, A. Chotia, M. Allegrini, N. Bouloufa, O. Dulieu, D. Comparat, and P. Pillet, *Science*, 2008, **321**, 232.
- [9] J. Deiglmayr, A. Grochola, M. Repp, K. Mörtlbauer, C. Glück, J. Lange, O. Dulieu, R. Wester, and M. Weidemüller, *Phys. Rev. Lett.*, 2008, **101**, 133004.
- [10] M. Aymar and O. Dulieu, *J. Chem. Phys.*, 2005, **122**, 204302.
- [11] A. Micheli, G. K. Brennen, and P. Zoller, *Nature Physics*, 2006, **2**, 341.
- [12] G. Pupillo, A. Griessner, A. Micheli, M. Ortner, D.-W. Wang, and P. Zoller, *Phys. Rev. Lett.*, 2008, **100**, 050402.
- [13] P. Rabl, D. DeMille, J. M. Doyle, M. D. Lukin, R. J. Schoellkopf, and P. Zoller, *Phys. Rev. Lett.*, 2006, **97**, 033003.
- [14] T. Zelevinsky, S. Kotochigova, and J. Ye, *Phys. Rev. Lett.*, 2008, **100**, 043201.
- [15] T. V. Tscherbul and R. V. Krems, *Phys. Rev. Lett.*, 2006, **97**, 083201.
- [16] S. D. Kraft, P. Staanum, J. Lange, L. Vogel, R. Wester, and M. Weidemüller, *J. Phys. B*, 2006, **39**, S993.
- [17] S. D. Kraft, J. Mikosch, P. Staanum, J. Deiglmayr, J. Lange, A. Fioretti, R. Wester, and M. Weidemüller, *Appl. Phys. B*, 2007, **89**, 453.
- [18] M. W. Mancini, A. R. L. Caires, G. D. Telles, V. S. Bagnato, and L. G. Marcassa, *Eur. Phys. J. D*, 2004, **30**, 105.
- [19] U. Schlöder, H. Engler, U. Schünemann, R. Grimm, and M. Weidemüller, *Eur. Phys. J. D*, 1999, **7**, 331.

- [20] W. Ketterle, K. B. Davis, M. A. Joffe, A. Martin, and D. E. Pritchard, *Phys. Rev. Lett.*, 1993, **70**, 2253.
- [21] C. G. Townsend, N. H. Edwards, K.P.Zetie, C. J. Cooper, J. Rink, and C. J. Foot, *Phys. Rev. A*, 1996, **53**, 1702.
- [22] K. M. Jones, E. Tiesinga, P. D. Lett, and P. S. Julienne, *Reviews of Modern Physics*, 2006, **78**, 483.
- [23] K. M. Jones, P. D. Lett, E. Tiesinga, and P. S. Julienne, *Phys. Rev. A*, 1999, **61**, 012501.
- [24] M. Marinescu, H. R. Sadeghpour, and A. Dalgarno, *Phys. Rev. A*, 1994, **49**, 982.
- [25] P. Sta anum, A. Pashov, H. Knöckel, and E. Tiemann, *Phys. Rev. A*, 2007, **75**, 042513.
- [26] M. Mudrich, S. Kraft, K. Singer, R. Grimm, A. Mosk, and M. Weidemüller, *Phys. Rev. Lett.*, 2002, **88**, 253001.
- [27] A. Stein, A. Pashov, P. Sta anum, H. Knöckel, and E. Tiemann, *Eur. Phys. J. D*, 2008, **48**, 177.
- [28] A. Grochola, A. Pashov, J. Deiglmayr, M. Repp, R. Wester, and M. Weidemüller, *In preparation*.
- [29] A. Grochola, J. Deiglmayr, R. Wester, M. Weidemüller, and O. Dulieu, *In preparation*.
- [30] A. Pashov, *private communication*.
- [31] V. Kokoouline, O. Dulieu, R. Kosloff, and F. Masnou-Seeuwsa, *J. Chem. Phys.*, 1999, **110**, 9865.
- [32] C. E. Moore, *Atomic Energy Levels, vol. III*, National Bureau of Standards, 1958.
- [33] L. V. Szentpaly, P. Fuentealba, H. Preuss, and H. Stoll, *Chem. Phys. Lett.*, 1982, **93**, 555.
- [34] M. Korek, A. Moghrabi, A. Allouche, and M. Aubert Frécon, *Can. J. Phys.*, 2006, **84**, 959.
- [35] S. Azizi, M. Aymar, and O. Dulieu, *AIP Conf. Proc.*, 2007, **935**, 164.
- [36] S. H. Patil and K. T. Tang, *J. Chem. Phys.*, 2000, **113**, 676.
- [37] L. Bellomonte, P. Cavaliere, and G. Ferrante, *J. Chem. Phys.*, 1974, **61**, 3225.
- [38] D. Wang, J. T. Kim, C. Ashbaugh, E. E. Eyler, P. L. Gould, and W. C. Stwalley, *Phys. Rev. A*, 2007, **75**, 032511.
- [39] J. Deiglmayr, M. Aymar, R. Wester, M. Weidemüller, and O. Dulieu, *J. Chem. Phys.*, 2008, **129**, 064309.
- [40] A. Mosk, S. Kraft, M. Mudrich, K. Singer, W. Wohlleben, R. Grimm, and M. Weidemüller, *Appl. Phys. B*, 2001, **73**, 791.

- [41] P. Staanum, S. D. Kraft, J. Lange, R. Wester, and M. Weidemüller, *Phys. Rev. Lett.*, 2006, **96**, 023201.
- [42] N. Zahzam, T. Vogt, M. Mudrich, D. Comparat, and P. Pillet, *Phys. Rev. Lett.*, 2006, **96**, 023202.
- [43] E. R. Hudson, N. B. Gilfoy, S. Kotochigova, J. M. Sage, and D. DeMille, *Phys. Rev. Lett.*, 2008, **100**, 203201.
- [44] A. V. Gorshkov, P. Rabl, G. Pupillo, A. Micheli, P. Zoller, M. D. Lukin, and H. P. Buchler, *Phys. Rev. Lett.*, 2008, **101**, 073201.